Title: Sediment-associated processes account for most of the spatial variation in ecosystem respiration in the Yakima River basin

Authors: Vanessa A. Garayburu-Caruso[1+*], Matthew Kaufman[1,2+*], Brieanne Forbes[1], Robert O. Hall Jr.[3], Maggi Laan[1], Xingyuan Chen[1], Xinming Lin[1], Stephanie Fulton[1], Lupita Renteria[1], Yilin Fang[1], Kyongho Son[1], James C. Stegen[1,4]

[1]Pacific Northwest National Laboratory, Richland, WA 99354
[2]Worcester State University, Worcester, MA 01602
[3]Flathead Lake Biological Station, University of Montana, Polson, MT 59860
[4]Washington State University, Pullman, WA 99163
[+] These authors contributed equally.
*Correspondence: vanessa.garayburu-caruso@pnnl.gov and mkaufman1@worcester.edu

Abstract: Hyporheic zones (HZ) contribute substantially to total stream ecosystem respiration (ER_{tot}). We rely on process-based models to understand HZ respiration at watershed scales and field-based estimates of ER_{tot} at reach scales. These emphasize different but related processes that have not been jointly explored. Here we evaluate the degree to which spatial variation in HZ respiration predicted via process-based models can explain spatial variation in field-estimates of ER_{tot} across 33 sites in the Yakima River basin (YRB). We found that HZ respiration predicted by process-based models did not explain spatial variation in field estimates of ER_{tot}. Our results indicate that sediment-associated processes hydrologically connected to the active channel explained most of the spatial variation of ER_{tot} in the YRB. 88% of sites showed that sediment-associated respiration contributed to 50% or more of ER_{tot}, while a few sites showed as little as 0% contribution. We propose that ER_{tot} is influenced by processes that integrate contributions from sediment components beyond the HZ, such as benthic algae and submerged macrophytes, which are key primary producers in rivers. We encourage conceptual and process-based models of ER_{tot} to integrate shallow HZ exchange with sediment-associated primary production as these provide more complete accounting of processes influencing ER_{tot}.

Introduction

River corridors contribute substantial amounts of carbon dioxide (CO_2) to the atmosphere[1]. Specifically, areas where groundwater and surface water mix (i.e., hyporheic zones, HZ) can contribute 3-96% of total ecosystem respiration[2–7]. These contributions are variable and are not well understood at a basin scale. Field experiments have estimated HZ respiration via extrapolations of sediment microcosms[8,9], as the difference between ecosystem and benthic respiration[2], or via end-member mixing analysis using in-situ solute concentration[3]. However, quantifying HZ respiration in the field across scales is difficult due to high spatial and temporal heterogeneity in hydrologic conditions and stream geomorphology. Currently, we rely on models like Networks with Exchange and Subsurface Storage (NEXSS)[10] and the River Corridor Model (RCM)[11–13] to predict the spatial variation of HZ respiration at watershed to basin scales. These and other watershed/basin scale models rely on physical stream characteristics (e.g., sediment texture, geomorphology, discharge) to estimate hydrologic exchange fluxes that, when paired to reaction network models, provide an estimate of HZ respiration rates[10–13]. While each of these models provide insights into spatial patterns of HZ respiration, they have not been explored in conjunction with field estimates of total stream ecosystem respiration.

Ecosystem metabolism and carbon (C) cycling in rivers have been widely studied via two key processes: C fixation (gross primary production, GPP) and organic C mineralization (ecosystem

respiration, ER)[14]. Field estimates of these processes are often derived from diel dissolved oxygen (DO) measurements that include the collective aerobic organisms (i.e., autotrophs and heterotrophs) and habitats (i.e., benthic, planktonic, and hyporheic zones), which together contribute to C cycling dynamics in streams and rivers[15]. Studying river metabolism allows for deeper understanding about food webs, energy fluxes, C and nutrient cycling, as well as predictions of ecosystem responses to environmental change[16–19].

River metabolism is influenced by several biotic and abiotic factors like light, flow, temperature, nutrients, and hydrogeomorphology[20–22]. Additionally, studies worldwide have evaluated how environmental factors like climate, elevation, and latitude impact aquatic ecosystems[1,23,24]. A recent study across 222 rivers in the United States shows that light availability and stream flow conditions govern spatial variation in both annual GPP and ER[25]. Additionally, a global assessment of river metabolism shows that GPP and ER increased with latitude and suggests that spatial variability of site characteristics like land use and vegetation are more influential than latitudinal temperature effects on river metabolism[26]. These studies identified metabolism drivers linked to chemical and biological processes across scales, yet they do not explicitly consider the role of hydrologic exchange, a fundamental process within reactive transport models that heavily influences HZ biogeochemistry. Thus, we lack conceptual understanding of the degree to which HZ respiration predicted via process-based models explains spatial patterns of field estimates of total stream ecosystem respiration (ER_{tot}) at a basin scale.

In this study, we test the hypothesis that spatial variation in HZ respiration predicted via process-based models explain the spatial variation of field-estimates of ER_{tot} across 33 sites within the Yakima River Basin (YRB). We examine the relative contributions of water column respiration (ER_{wc}), and sediment associated respiration (ER_{sed}) to ER_{tot} to test the additional hypothesis that ER_{tot} is driven primarily by contributions from ER_{sed}, and less so by contributions from ER_{wc}. Upon finding that ER_{sed} usually accounts for most of ER_{tot}, we further investigate spatial drivers of ER_{sed} across the basin. Our study highlights the importance of sediment-associated processes for understanding basin scale spatial variability of ER_{tot} and emphasizes the need for process-based forward-simulation capabilities that incorporate multiple components of the river corridor, including water column processes, sediment-associated autotrophic and heterotrophic metabolism in benthic zones and HZs, and hydrologic exchange.

Results and Discussion

Our study provided three primary outcomes: (*i*) Spatial variation in model-predicted HZ respiration (as viewed through the river corridor model, RCM) did not explain spatial variation in field-estimates of stream ecosystem respiration (ER_{tot}) at the basin scale. (*ii*) Contributions from water column respiration (ER_{wc}) and sediment-associated respiration (ER_{sed}) were highly variable and ER_{sed} was the primary contributor to ER_{tot} across most sites. (*iii*) variation in ER_{sed} was primarily explained by gross primary production (GPP) and parameters reflecting the physical environment. These results suggest that there are processes driving spatial variation in ER_{tot} at a basin scale beyond those present in the RCM. We also infer there are processes in the RCM that may not be captured in field estimates of ER_{tot}. Our results provide guidance for which processes could be included in process-based models, such as the RCM, to support research efforts focused on understanding basin scale patterns and dynamics of ER_{tot} and ER_{sed}.

Spatial variation in RCM-predicted HZ respiration did not explain spatial variation in field-estimates of ER_{tot} across the YRB.

Estimates of time averaged ER_{tot} for the deployment period across sites (n = 45) was highly variable and ranged from -21.50 to 9.26 g O_2 m^{-2} day^{-1} (Fig. 1a). We could not estimate metabolism (i.e., GPP and ER_{tot}) in 3 sites that failed to meet the assumptions of one station open channel O_2 budgets due to slower flows and lack of turbulence[27]. In addition, out of the 45 sites where we were able to estimate metabolism, 12 sites displayed positive estimates of ER_{tot}. These had dissolved O_2 (DO) that rarely went under 100% saturation, which indicates high gas exchange rates potentially due to too much turbulence and bubbles at higher internal pressure relative to the atmosphere[28]. Oversaturation hinders the estimation of ER_{tot} using open channel DO time series because we have no simple way of knowing what the concentration of DO would be in the river in the absence of any biological activity[29]. We removed sites with positive ER_{tot} values from our analysis because they have no biological meaning, and their magnitude reflects misspecification due to bubble-mediated gas exchange and not a biological process. After removing these values, estimated time averaged ER_{tot} (n = 33) ranged from -21.50 to -0.12 g O_2 m^{-2} day^{-1}.

Field-estimates of ER_{tot} diverged from RCM-predicted HZ respiration, both quantitatively and qualitatively. The fastest ER_{tot} rates occurred in the lower region of the YRB (Fig. 1a), in locations with shallow topographic gradients and high order streams (i.e., topographic slopes of 0.0004 - 0.002 and stream orders of 5-7). The fastest HZ respiration rates predicted by the RCM were, in contrast, in upper parts of the YRB (Fig. 1b). RCM-predicted HZ respiration values (n = 46) ranged from -800 to -0.024 g O_2 m^{-2} day^{-1}. The RCM-predicted rates were much faster than estimates of ER_{tot} highlighting fundamental differences in the processes represented in the RCM vs. processes that influence ER_{tot} field estimates. Adding processes to the RCM or making inferences regarding quantitative differences in the rates is beyond the scope of the current study. We instead use RCM-predicted spatial patterns as the best current representation for spatial patterns in HZ respiration rates across the YRB. This approach allows for evaluating a qualitative relationship between the spatial patterns of RCM-predicted HZ respiration and field-based ER_{tot}.

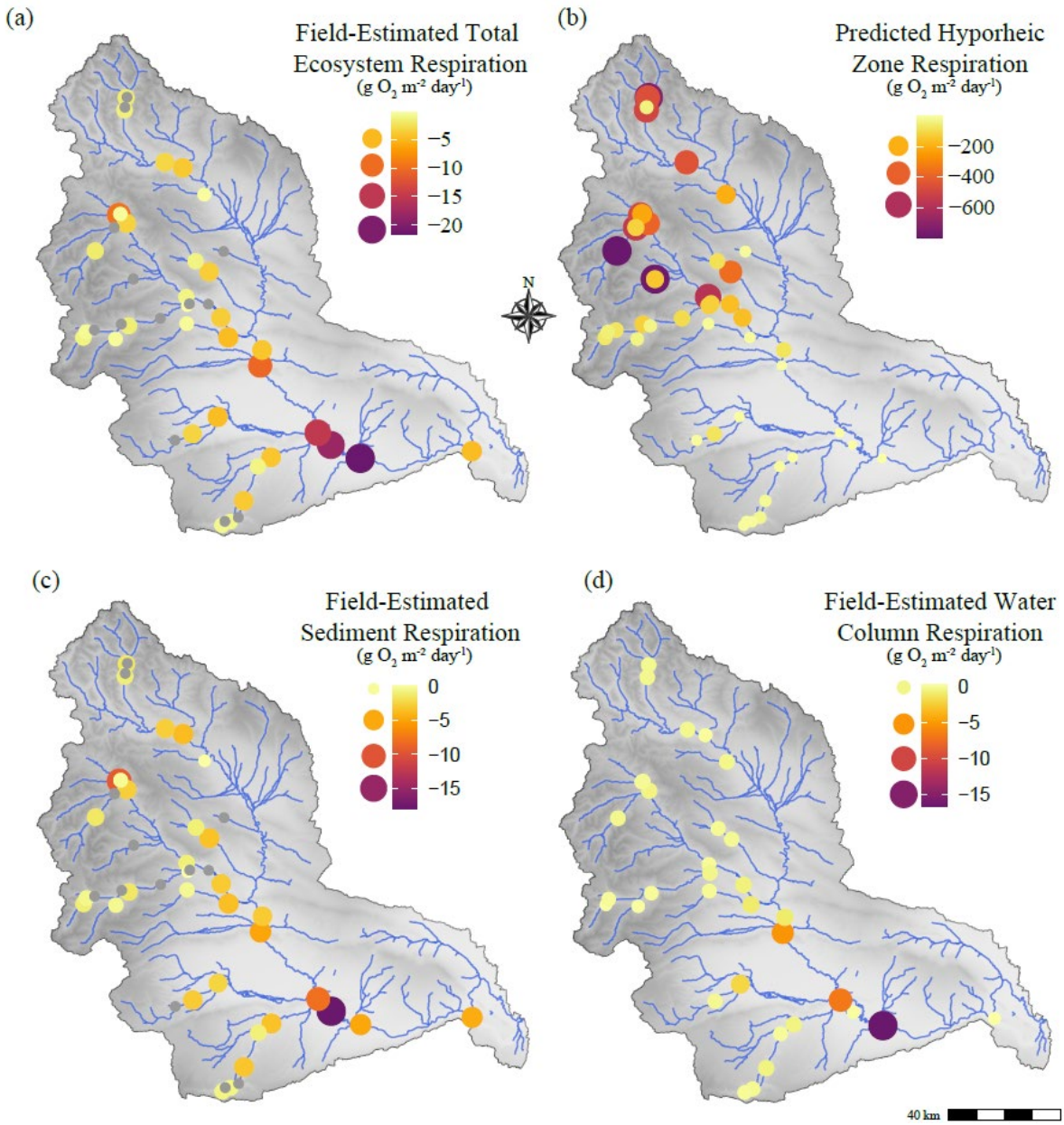

Figure 1. Map displaying Yakima River basin sites investigated in this study and associated respiration rates. (a) Field-estimates (n = 48) of total stream ecosystem respiration rates (ER_{tot}). (b) River Corridor Model (RCM, n = 46) predicted hyporheic zone (HZ) respiration rates[13]. (c) Field-estimates (n = 48) of sediment-associated respiration rates (ER_{sed}). (d) Field-estimates (n = 48) of water column respiration rates (ER_{wc}). Color and symbol size are used to indicate magnitude of respiration rate. Grey dots in panels a and c indicate sites where ER_{tot} or ER_{sed} could not be estimated or where ER_{tot} was positive.

Spatial variation in RCM-predicted HZ respiration had a weak negative relationship with spatial variation in ER_{tot}. Before doing associated analyses and given the quantitative difference between RCM predictions and ER_{tot}, we standardized rates within each dataset as z-scores, whereby each dataset has a mean of zero and standard deviation of one. This does not change quantitative relationships within each dataset or the shape of the data distribution, it only puts the two datasets into the same quantitative scale. Following this normalization, we regressed RCM-predicted HZ respiration z-scores against z-scores of field-estimates of ER_{tot} (Fig. 2). These data violated the normality assumption for conducting a parametric regression, yet no

relationship is apparent in the data (Fig. 2a). A weak negative relationship was, however, observed via Spearman rank-order correlation (Fig. 2b). The negative direction and weakness of the relationship indicate, however, that HZ respiration—as represented in the RCM—is not a primary factor explaining spatial variation of ER_{tot} in the YRB. The lack of a strong positive relationship could be for several reasons, such as ER_{tot} not including respiration occurring across the full HZ spatial domain that is represented in the RCM, and the RCM not including all the river corridor components and drivers influencing ER_{tot} estimates.

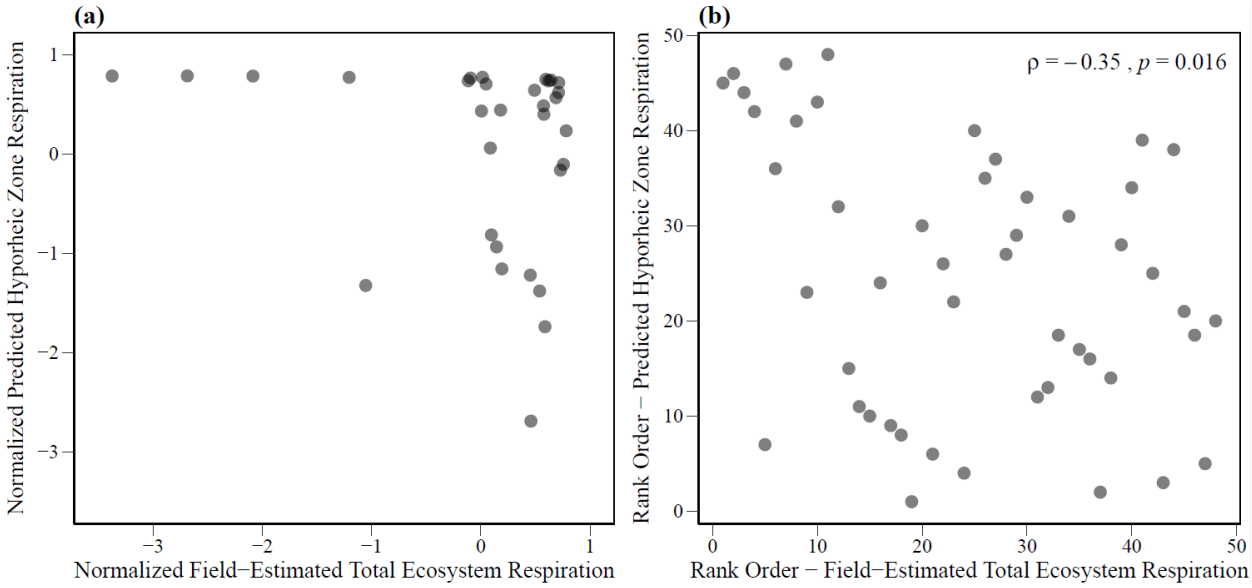

Figure 2. Normalized model-predicted hyporheic zone (HZ) respiration rates do not increase with field-estimates of total stream ecosystem respiration rates (ER_{tot}; n = 31). (a) Z-score normalized data suggest no relationship. Data distributions are skewed (i.e., not normal) and thus violate assumptions of parametric regression, so no statistics are given. (b) Spearman rank-order correlation reveals a weak, negative relationship. The Spearman correlation statistics are provided on the panel.

Field-estimates of ER_{tot} are based on DO dynamics that reflect the reach-scale integrated outcome of processes occurring across all system components that are hydrologically connected to the active channel[15]. This estimate includes respiration associated with subsurface sediments along relatively short HZ flow paths. These HZ flow paths must be fully contained within the upstream reach that influences observed DO dynamics at a given monitoring location. If the HZ flow paths are longer, they should not influence observed DO and thus do not influence estimated ER_{tot}. The length of the reach that a given DO sensor integrates varies across streams and has been estimated to be roughly three times the turnover length of O_2[15]. It is plausible that the RCM captures respiration along flow paths that are longer and deeper into the HZ than what the DO sensors integrate across. If so, respiration in long flow paths—that are captured in the RCM—could lead to the lack of positive correlation between RCM-predicted HZ respiration and field-estimates of ER_{tot}. We suspect, however, that this might not be the primary reason for the lack of a relationship because both RCM-predicted HZ respiration and field-estimates of ER_{tot} account for short HZ flow paths. These shorter flow paths are likely to be within the most biogeochemically active sediments, which should in turn be the primary drivers of total HZ respiration[30]. We postulate that the lack of a relationship (Fig. 2) and divergence in spatial patterns (Fig. 1a, b) is related to differences in which biogeochemical processes are captured in the two methods.

The RCM represents hydrologic exchange through the HZ and sediment-associated respiration that is fueled by reactants delivered by that exchange[13]. In the model, reactants delivered to HZ

sediments are not influenced by primary producers (e.g., photoautotrophic algal biofilms) and the respiration contributed by primary producers is also not accounted for. Respiration occurring by heterotrophs and photoautotrophic primary producers in the water column is also not part of the RCM. All these processes can influence observed DO dynamics[31–33] and are thus implicitly accounted for in field-estimates of ER_{tot}. This highlights that field estimated ER_{tot} is influenced by several processes that are not represented in the RCM. This is not a critique or rejection of the RCM, rather, it is a recognition that the divergence in spatial patterns between RCM-predicted HZ respiration and field-estimates of ER_{tot} are likely due, at least in part, to a difference in the processes captured by each method.

In addition to the differences in captured processes, RCM-predicted HZ respiration and ER_{tot} may not be correlated if processes in the RCM do not strongly influence ER_{tot}, if data inputs to the RCM misrepresent the system, or if there are technical issues associated with estimating ER_{tot}. Sites with technical issues were removed from the analysis and our estimates of ER_{tot} largely overlap with literature values[25,34] (Fig. 3a). It is, therefore, likely that the ER_{tot} estimates represent actual stream respiration suggesting that technical issues with the estimates are not a cause for the lack of correlation. Thus, the lack of correspondence in spatial patterns suggests that to use the RCM, or other processed-based models, in future studies to help understand ER_{tot} it may be useful to expand the breadth of represented processes. Available field estimates of ER_{tot} allow us to guide which processes could be most important to include in the RCM and, more generally, to investigate factors associated with spatial patterns in ER_{tot}. To these ends, we next examine the relative influence of water column- and sediment-associated processes over ER_{tot}, which provides conceptual understanding of system function and evaluates the need for each of these in an expanded version of the RCM.

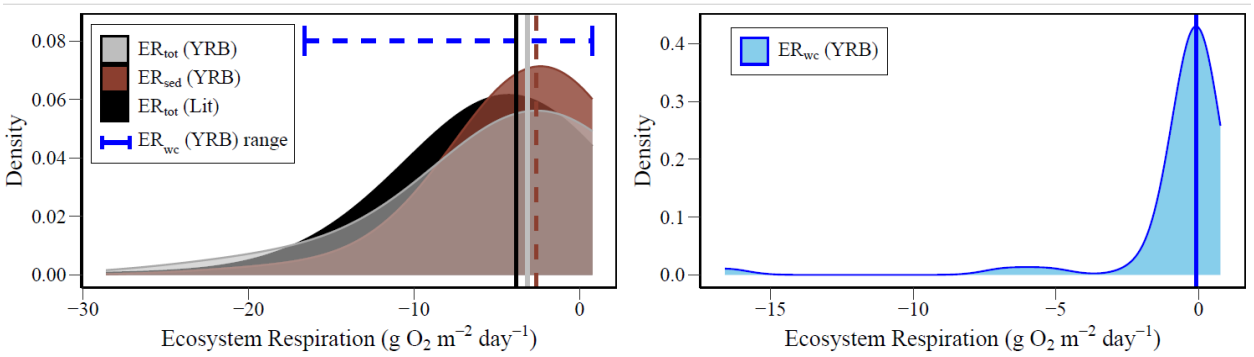

Figure 3. Density plots comparing respiration rates for different river corridor components within the Yakima River basin (YRB) as well as literature values. (a) Density plot for YRB total ecosystem respiration from this study (ER_{tot}, grey, n = 33) and from rivers and streams across the Contiguous United States (CONUS) (n = 222 estimated by Appling et al.[34] and Bernhardt et al.[25] (ER_{tot}(Lit), black), as well as YRB ER_{sed} (brown, n = 33) and the range of YRB water column respiration rates (ER_{wc}, blue n = 48); (b) Density plot for YRB ER_{wc} (blue). The vertical lines are the medians for each distribution.

The spatial distribution of ER_{tot} was largely explained by variations in ER_{sed} with limited influence from ER_{wc}.

Our ER_{wc} data, estimated via *in-situ* dark bottle incubations (n = 48) varied greatly across the basin and ranged from -16.60 to +0.772 g O_2 m^{-2} day^{-1} (Fig. 3b). Contrary to the data cleaning decisions made for ER_{tot}, we chose to interpret positive ER_{wc} because they reflect instrument noise paired with extremely slow respiration. In this situation the rate at which O_2 was consumed was not fast enough to overcome instrument error and resulted in a small positive ER_{wc}

measurement. If these values were excluded it would bias the dataset away from locations with very slow ER_{wc} rates. Across all 33 field locations with ER_{tot} estimates, ER_{wc} varied greatly and had fractional contributions of ER_{wc} to ER_{tot} spanning 0-100% (Table 1, Fig. S1a). The range of measured ER_{wc} values spans a substantial portion of ER_{tot} literature values (Fig. 3a). These results highlight the diversity of environments in the YRB and suggests that ER_{wc} can be of similar magnitude to ER_{tot} across Contiguous United States (CONUS) rivers.

Table 1. Summary statistics (mean, median, and range) for ER_{tot} (g O_2 m^{-2} day^{-1}), ER_{wc} (g O_2 m^{-2} day^{-1}), ER_{sed}, (g O_2 m^{-2} day^{-1}), and ER_{wc} and ER_{sed} contributions to ER_{tot} (percent).

	Mean	**Median**	**Range**
ER_{tot}	-4.14	-3.15	(-21.50, -0.12)
ER_{wc}	-0.725	-0.0845	(-16.60, 0.772)
ER_{sed}	-3.05	-2.62	(-17.96, 0)
ER_{wc} (%)	8.4%	17.7%	(0%,100%)
ER_{sed} (%)	82.3%	91.7%	(0%, 100%)

Spatial patterns in ER_{wc} showed some similarity to spatial patterns in ER_{tot} (Fig. 1a, d, Fig. S1b). As discussed in Laan et al.[35], ER_{wc} in the YRB spans values that are similar to other streams and rivers around the world[36–38]. Variable ER_{wc} rates in the YRB could be due to variable amounts of total suspended solids (TSS), nutrient concentrations, and changes in depth and surface water residence time, moving from headwaters to larger order streams[35,36,39]. Moreover, our results indicate that respiration contributions from ER_{wc} can vary widely across the YRB during base-flow conditions. Within the YRB, 4 locations had ER_{wc} that contributed more than 50% of ER_{tot}. We observed the largest contribution of ER_{wc} to ER_{tot} in 4th and 5th order streams, which were also the locations with the slowest ER_{tot}. While ER_{wc} and ER_{tot} rates at these locations were slow, the water column was responsible for all the observed respiration. These findings align with previous studies finding large ER_{wc} contributions. For example, working in mid-sized rivers, Reisinger et al.[38] found that ER_{wc} contributed an average of 35% to ER_{tot}, and up to 81% in rivers with slow ER_{tot}. Similarly, the rates of other water column processes, like nutrient uptake and denitrification, may increase with increasing river size, as material processing shifts from being benthic-dominated to water-column dominated in rivers from 5th to 9th order[40–43]. These patterns suggest that the relative importance of ER_{wc} is governed by several stream characteristics, some of which co-vary with stream order.

We further examined respiration contributions from river corridor components beyond the water column (i.e., benthic/streambed sediments and HZs that are hydrologically connected to the active channel). We define the respiration that comes from these integrated components as sediment-associated respiration (ER_{sed}). ER_{sed} was calculated as the difference between ER_{tot} and ER_{wc} at each site with negative ER_{tot} (n = 33) assuming zero ER_{wc} rates if ER_{wc} values were positive (n = 12). ER_{sed} values ranged from -17.96 to 0 g O_2 m^{-2} day^{-1} (Table 1). The relative contribution of ER_{sed} to ER_{tot} spanned from 0-100%, with 29 out of 33 locations (88% of locations) showing ER_{sed} contributions exceeding 50% of ER_{tot} (Table 1, Fig. 4a). The strong contribution of ER_{sed} to ER_{tot} across the YRB aligns with previous studies that have found large contributions of HZ and benthic sediments to ecosystem respiration[3,44–46]. It is important to note that our ER_{sed} measurements integrate multiple ecosystem components, including the HZ, benthic biofilms, and submerged macrophytes, whereas ER_{wc} specifically represents respiration from organisms suspended in the water column.

ER_{sed} accounted for most of the spatial variability in ER_{tot} across the YRB (Fig. 1a,c). However, no spatial correlation was observed between ER_{sed} and RCM-predicted HZ respiration (Fig. S2). While ER_{sed} was fastest in lower parts of the YRB, the RCM predicted fastest HZ respiration in upper parts of the YRB (Fig.1b, c). The correspondence between ER_{sed} and ER_{tot} spatial patterns reflected the dominant contribution of ER_{sed} to ER_{tot} (Fig. 4b). This finding is consistent with previous studies across different stream orders. For example, Naegeli and Uehlinger[2] found that ER_{sed} contributed 76–96% of ER_{tot} in a gravel bedded river using closed chamber measurements. Similarly, Fellows et al.[9] reported large HZ contributions to ER_{tot} (40-93%) in two headwater streams under baseflow conditions. In contrast, Battin et al.[3], found lower HZ contributions (41% of ER_{tot}) in a third-order piedmont stream, while Roley et al.[47] observed that water column processes dominated ER_{tot} in the mainstem Columbia River (9th order river). These varying results, together with our findings, demonstrate that ER_{sed} contributions can span a wide range across river networks. While these studies provide valuable insights into specific stream reaches, they highlight a critical knowledge gap in our understanding of what drives ER_{sed} variability at the basin scale. Our dataset from the YRB provides a useful opportunity to investigate potential drivers of spatial variation in ER_{sed} across an environmentally diverse river network.

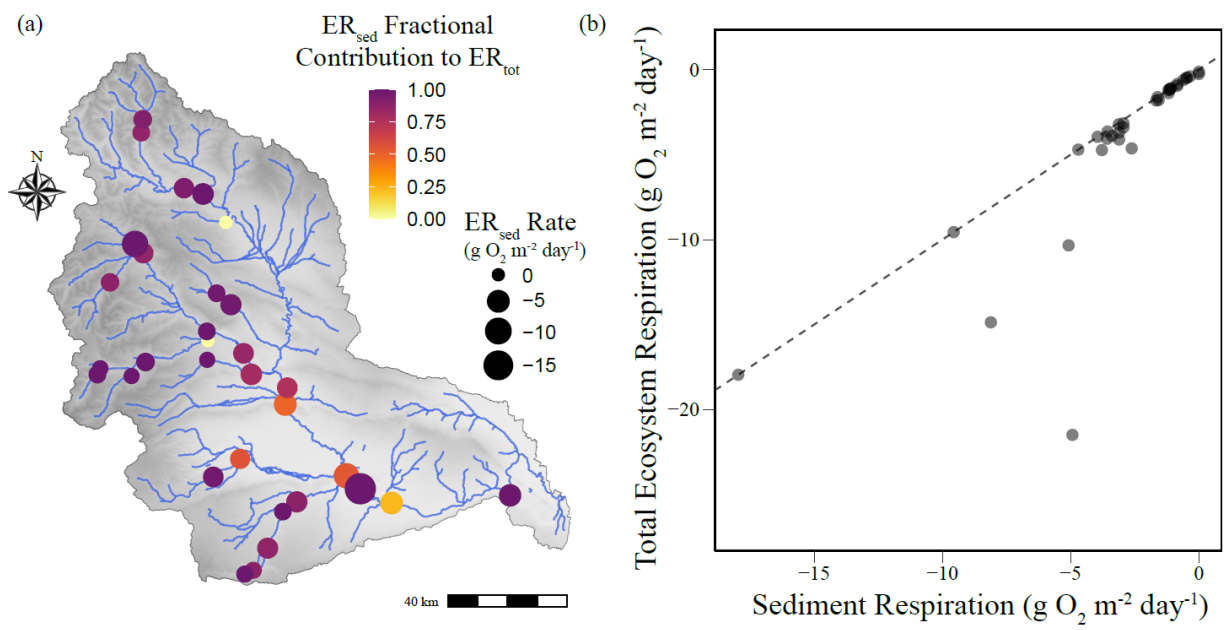

Figure 4. ER_{sed} contributions to and correspondence with ER_{tot}. (a) Map displaying the fractional contributions of sediment-associated respiration (ER_{sed}) to total ecosystem respiration (ER_{tot}) across the YRB (n = 33). Color is used to indicate the magnitude of the fractional contribution while symbol size is used to indicate magnitude of ER_{sed} respiration rate. (b) Scatterplot relating ER_{tot} to ER_{sed}. The grey dashed line is the one-to-one line.

Spatial variability in ER_{sed} was best explained by primary production and physical settings.

To investigate factors explaining spatial variation in ER_{sed}, we identified variables known from previous work to influence ER_{tot} (e.g., gross primary production; GPP) and variables that influence HZ respiration (e.g., median grain size). We did not include RCM-predicted HZ respiration as an explanatory variable because it was strongly correlated with median grain size (i.e., d50), and because we did not find a positive relationship between RCM-predicted HZ

respiration and ER_{tot} or ER_{sed} (Fig. 2, Fig. S2). Our analysis showed that GPP, stream slope, stream velocity, and total dissolved nitrogen (TDN) explained the most variation in ER_{sed} (Table 2). Other potential drivers (i.e., land cover classes, median grain size, nutrients, depth and water temperature) had smaller regression coefficients (< 0.1) and were interpreted as being not as important. The directionality of these relationships further showed that the fastest ER_{sed} rates (and thus ER_{tot} rates) had the fastest GPP rates (Table 2). This finding is generally consistent with the observation from Bernhardt et al.[25] who found that ER_{tot} was most strongly linked to light availability, which should influence GPP. Additionally, faster ER_{sed} rates were observed in reaches with shallower topographic gradients, lower velocity, and higher TDN concentrations. Flow velocity controls biofilm scouring, architecture, and functional dynamics[48,49]. Moreover, stream slope influences flow velocities, sediment transport[50], and nitrogen concentrations, which can all impact biofilm community structure and C uptake[51]. Together these variables can have a substantial effect on benthic metabolism and in turn ER_{sed}.

Table 2. Regression coefficients for LASSO models explaining variation in ER_{sed}. All input variables from 33 sites were cube root transformed to reduce the impact of high leverage points in the regression analysis and standardized as z-scores to enable direct comparison of the regression coefficients. The LASSO regressions were performed over 100 seeds. Reported mean regression coefficients (β) and R^2 were averaged across the 100 seeds. Normalized regression coefficients were calculated by dividing each β coefficient by the maximum β coefficient in each seed. Standard deviation (sd) was calculated for each coefficient over the 100 seeds. Values of 0 indicate that the variable was included as an input to the model but not assigned a β coefficient.

Input Variable	**Mean Normalized Regression Coefficient (β)**	**sd**	**Mean Regression Coefficient (β)**	**sd**
Slope	1	0	0.293	0.014
Gross Primary Production	-0.697	0.014	-0.204	0.006
Velocity	0.631	0.029	0.185	0.017
Total Dissolved Nitrogen	-0.441	0.027	-0.129	0.003
Percent Agricultural Cover	0.003	0.025	0.001	0.009
Percent Forest Cover	0.003	0.021	0.001	0.007
Percent Shrub Cover	0.002	0.015	0.001	0.005
Drainage Area	0	0	0	0
Aridity	0	0	0	0
Discharge	0	0	0	0
Median Grain Size	0	0	0	0
Total Suspended Solids	0	0	0	0
Dissolved Organic Carbon	0	0	0	0
Mean Depth	0	0	0	0
Water Temperature	0	0	0	0
Mean R^2				**0.52 (sd = 0.008)**

In addition, ER_{sed} and ER_{tot} covaried linearly with GPP (Fig. 5) providing insight into net ecosystem production and the metabolic balance of the stream. This information can be discerned by examining the position of sites relative to the one-to-one line in Fig. 5, where points below the line indicate net heterotrophy and points above the line indicate net autotrophy. Our results showed that 22 sites were net autotrophic and 11 sites were net heterotrophic. This finding contrasts the general paradigm that stream ecosystems are predominantly heterotrophic, where respiration is sustained by allochthonous C inputs, making rivers net sources of CO_2 to the atmosphere[15,17,25,52,53]. In autotrophic conditions, rivers fix more carbon than they respire,

potentially storing or exporting this excess carbon downstream[15]. Larger number of sites exhibiting net autotrophy in the YRB might be due to summer baseflow conditions when light availability is maximized, combined with stable flow conditions that promote primary production[54]. Similar patterns of autotrophy have been observed during baseflow in agricultural systems[55], montane streams with some seasonal and year-to-year variability [56], and managed pastoral streams[57].

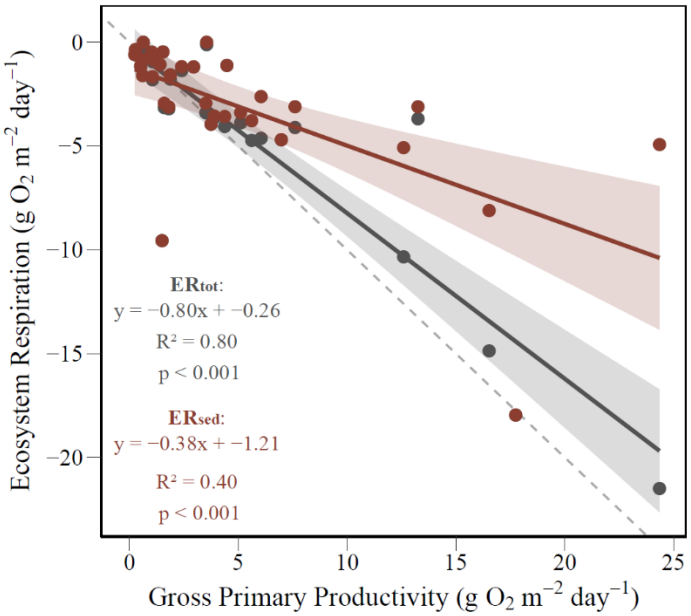

Figure 5. ER_{sed} and ER_{tot} as a function of GPP. Scatterplot with linear regression lines depicting the relationship between GPP (x-axis) and field estimates of sediment respiration (ER_{sed}, brown, y-axis) and field estimates of total respiration (ER_{tot}, dark grey, y-axis). The grey dashed line is the one-to-one line with slope of –1.

The relatively large LASSO coefficient for GPP (the largest coefficient after slope, Table 2), and faster ER_{sed} (more negative) with increasing GPP (Fig. 5), suggest an important link between sediment-associated primary production and ER_{sed}. Primary producers in this case are likely to include both algal biofilms attached to benthic/streambed sediments and submerged macrophytes rooted in sediments. We infer that both types of primary producers likely provide important direct and indirect contributions to ER_{sed}. Direct contributions include phototroph respiration, and indirect contributions include providing resources (e.g., organic exudates) to sediment-associated heterotrophs[14,58]. This link between ER_{sed} and GPP in the YRB is conceptually consistent with Bernhardt et al.[25]'s result that light is a primary explanatory variable for ER_{tot} across CONUS. Further consistent with Bernhardt et al.[25] is our result that ER_{sed} rates (and thus ER_{tot} rates) are likely influenced by variables beyond GPP that may be linked to hydrologic exchange. In the YRB, low-gradient reaches with slow moving water had faster ER_{sed} (Table 2). This relationship may additionally reflect a shift along the transporter-to-transformer continuum[59–61] whereby residence time is long enough to enable significant reactions to occur, thereby enhancing ER_{sed}. Together, these results point to a key role for the ratio of residence time to reaction time as classically represented in the Damköhler number[62]. That is, we infer that ER_{sed} hot spots[63] or control points[64] are more likely to occur when the Damköhler number is high because of low gradient and slow flow causing long residence time and fast GPP causing short reaction times. These factors are likely predictable from physical features of stream networks, thereby providing opportunities to develop mechanistic or data-driven models of ER_{sed} hot spots/control points.

Conclusions

Spatial patterns of ER_{sed} largely corresponded to ER_{tot} patterns, thus understanding basin-scale ER_{tot} requires deeper understanding of controls on ER_{sed} spatial variability. Our analysis revealed that ER_{sed} across the YRB was primarily explained by slope, GPP, velocity and TDN with the fastest ER_{sed} rates occurring in reaches characterized by high GPP, gentle slopes, slower velocities, and elevated TDN concentrations. This relationship suggests a complex coupling between physical, chemical, and biological drivers linked to sediment-associated primary production and the transporter-to-transformer continuum. Further, the lack of positive correlation between RCM-predicted HZ respiration and field-estimates of ER_{sed} and ER_{tot} highlights a need to extend conceptual and process-based models that aim to capture and predict active channel respiration to represent all processes that have major influences over those rates. The RCM relies heavily on several spatially variable inputs, including median grain size (i.e., d50) and dissolved organic carbon (DOC) concentrations. These input data layers, particularly d50, are generated from sparse field measurements and may not accurately reflect local conditions in the basin. If the spatial patterns in d50 within the input data deviate from true spatial patterns in d50, that will cause errors in predicted spatial patterns of HZ respiration. Additionally, the model does not consider the impact of sediment grain size on reaction rates, only on exchange rates.

To understand spatial patterns in ER_{tot} and ER_{sed} we propose that it is not enough to focus on HZ respiration as influenced primarily by hydrologic exchange processes. Our results indicate a need to explicitly represent primary producers and heterotrophs in both the water column and associated with sediments. Current models can be modified in these ways to generate new predictions for evaluation with further field deployments designed specifically to test them. We refer to this approach as hypothesis-based model-experiment (ModEx) iteration, and this study represents a key step in this approach. A ModEx approach goes beyond data-model integration whereby models are used to pose new hypotheses that are tested with new data, leading to modified hypotheses that guide follow-on model development, and so on. We encourage the application of this approach in other basins and across other flow conditions to evaluate the transferability of our outcomes. This is key to building predictive models that are useful across Earth's diverse watershed systems.

Methods

1. Site selection

We selected the Yakima River basin (YRB) as a test basin for this study. The basin drains an area of 15,941.4km^2 and spans forested mountainous regions in the west to arid valleys and plains in the east (Fig 6). The basin has a diversity of land covers and land uses dominated by dry rangeland, forest, and agriculture[65,66]. Annual precipitation ranges from 203-356 cm in the west to 25 cm in the east[67].

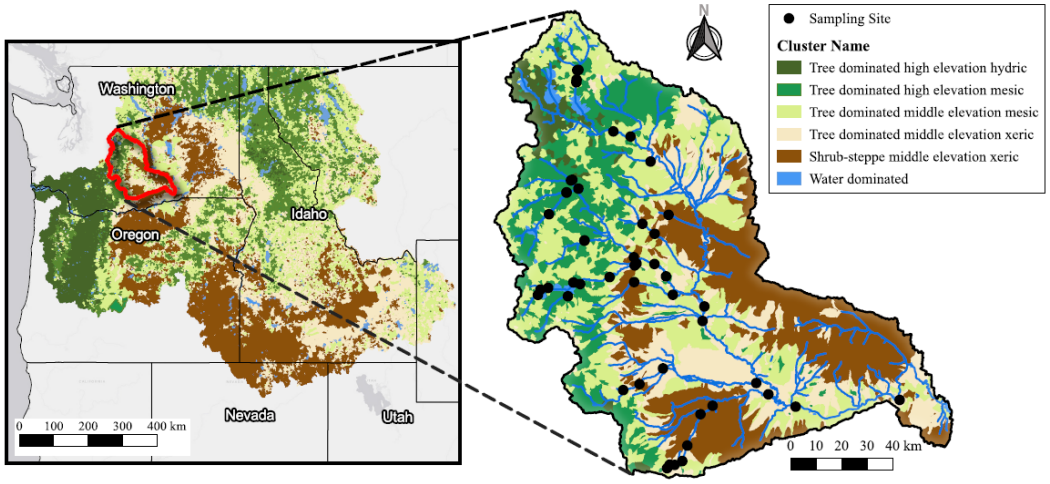

Figure 6. Yakima River basin sampling sites superimposed on a map of catchment cluster analysis results.

Field sites spanned a range of stream orders, land cover types, physical settings, and previously published model-predicted HZ respiration rates[13]. Because model-predictions were performed at a reach scale for the Columbia River basin, we conducted a clustering analysis following methods previously described by Laan et al.[35] to locate regions in our test basin with representative characteristics from the Columbia River basin (Fig. 6). We then combined the clustering analysis results with logistical considerations regarding site access, safety, and model-predicted HZ respiration rates to select 48 sites that span a range of clusters, model-predicted respiration rates and stream orders across the basin (Fig. 6). Table 3 shows a summary of the cluster analysis results as well as number of sites in the YRB per cluster. Geospatial variables for each site were extracted primarily from the Environmental Protection Agency StreamCat Dataset and NHDPlusV2.1 using a custom R script[68]. Land use/land cover data for all the sites were extracted from StreamCat [69], while catchment area and slope were extracted via NHDPlusV2.1 with the R package 'nhdplusTools'[70]. The custom R script was also used to extract aridity data from the Global Aridity Index and Potential Evapotranspiration (ET0) Database: Version 3[71] with the terra::rast() and terra::extract() functions[72].

Table 3. Cluster analysis results across the Columbia River basin and Yakima River basin with similar biophysical and hydrologic characteristics and the number and percentage of sites in each.

Cluster	Cluster Name	CRB Drainage Area (%)	YRB Drainage Area (%)	No. YRB Sites Per Cluster	Percent YRB Sites Per Cluster (%)
1	Tree dominated high elevation mesic	22.7	27.4	12	25.0
2	Water dominated	3.4	2.2	0	0
3	Tree dominated high elevation hydric	7.3	2.4	2	4.2
4	Shrub-steppe middle elevation xeric	25.4	28.1	5	10.4
5	Tree dominated middle elevation mesic	17.4	17.3	15	31.3
6	Tree dominated middle elevation xeric	23.9	22.6	14	29.2

"CRB Drainage Area" is the percentage of the total drainage area of the Columbia River basin that was classified in each cluster. "YRB Drainage Area" is the percentage of the total drainage area of the Yakima River basin that was classified in each cluster. "YRB Sites Per Cluster" is the total number of field sites in the Yakima River basin (n = 47) located in each cluster. "Percent YRB Sites Per Cluster" is the percentage of the total number of sampling sites in the Yakima River basin located in each cluster.

2. Sensor deployment and data collection

During the week of July 25–28, 2022, dissolved oxygen (DO) sensors (miniDOT Logger; PME, Inc.; Vista, CA, USA) and level loggers (HOBO® Water Level Logger (13') U20L-04; Onset; Bourne, MA, USA) were deployed with sensor windows facing upstream on the thalweg of the riverbed at each site (n = 48) for 35 days during baseflow conditions. We were unable to deploy sensors and sample first order streams due to the lack or low flow during the summer. The sensors were secured to two bricks with zip ties using several different configurations depending on streamflow velocity, depth, and channel substrate (Fig. 7b, d). DO sensors recorded DO and water temperature continuously on a 1-min interval. To minimize sensor biofouling in warmer, shallower rivers or rivers that received a lot of sunlight, 25 DO sensors were equipped with wipers (miniWIPER for miniDOT; PME; Vista, CA, USA) and anti-fouling copper plates (miniDOT Anti-fouling Copper Option; PME; Vista, CA, USA) (Fig 7d). Wipers were programmed to wipe the sensor face once every 12 hours. The remaining 23 DO sensors were equipped with full copper kits, which included a copper ring, silicone ring, and a copper mesh (Fig. 7b). Non-vented level loggers recorded absolute pressure and water temperature continuously on a 15-min interval. Additional barometric pressure (BP, Rugged BaroTROLL Data Logger (9 m); In-Situ; Fort Collins, CO, USA) sensors were deployed at a subset of sites (n = 9) to collect continuous BP and air temperature data throughout the study period (Fig. 7). Sensors were deployed from a 1-m rope on a tree branch as close as possible to the DO sensor/level logger deployments and recorded BP and air temperature continuously on a 1-min interval. BP data was used convert level logger absolute pressure data to depth data (Supplementary methods).

Level loggers and BP sensors were calibrated by the manufacturer and did not need further calibration. DO sensor calibrations were verified at 100% oxygen saturation in the laboratory prior to deployment and field-based data were corrected for sensor drift by applying a correction factor using lab-generated data (Supplementary methods). Approximately mid-way through the sampling period (August 8–11, 2022), sensors were field-checked for signs of disturbance, exposure due to decreased flows, and biofouling. DO sensors and level loggers were retrieved temporarily for maintenance and data downloads and immediately redeployed in the original location or, if exposed by decreasing flows, redeployed closer to the channel thalweg. Sensors were retrieved the week of August 29–September 1, 2022, and taken to the laboratory for data download.

Figure 7. Example sensor deployment configurations on example study sites. Left panels emphasize the diversity of environmental settings covered in this study. Right panels show two different sensor configurations used to accommodate different environmental conditions. (a) Bull Creek (site S63P), Yakama Reservation, Yakima County, Washington, 25 July 2022. (b) DO sensor and level logger deployed side-by-side on top of two bricks and secured with zip ties, 29 August 2022. DO sensor equipped with an anti-biofouling copper plate and mesh to inhibit the growth of periphyton on the sensor face. Note the dense accumulation of periphyton and sediment deposited on the sensor bodies and bricks. (c) Cle Elum River (site S24R) upstream of Cle Elum Lake, Kittitas County, Washington, 11 August 2022. (d) Level logger (far right) and DO sensor equipped with a wiper kit (white sensor body on left-hand side) and anti-biofouling copper plate, 01 September 2022. The white sensor body on the left-hand side of the wiper kit controls the blue flywheel, which is equipped with a brush and programmed to wipe the sensor face 1× every 12 h. Note the lighter accumulation of periphyton and sediment on the equipment deployed in the Cle Elum River (d) compared to the equipment deployed in Bull Creek (b).

3. Channel depth, channel width, and discharge data collection

Depth data for sites located on wadeable streams (n = 39) was collected using wading-based depth transects. For each desired reach length (Supplementary methods), we completed 5-10 depth transects over a period of one hour (a minimum of five transects was desired) using 2-person teams, starting ~2 m upstream of the depth sensor. Transects were evenly distributed along the length of the reach. Using a wading rod, depth measurements were collected along the wetted width of the reach at five roughly equidistance points along a transect perpendicular to flow. Field personnel manually recorded the start time and the coordinates for the starting point of each transect; the end time of the last transect was also manually recorded. The channel width of each transect was measured using a range finder; mean channel width was calculated by taking the average of the range finder width measurements.

Depth data for sites located on non-wadeable rivers (n = 5) was collected using kayak- or jetboat-mounted sonar (HDS-7 LIVE fish finder with Active Imaging™ 3 in 1 transducer; Lowrance; Tulsa, Oklahoma, USA) or, in the case of very large or inaccessible rivers (n = 4), publicly available gauging station data. Kayak-mounted sonar data was collected along each non-wadeable reach by 3-person kayak teams using a sonar receiver mounted to the bottom of a fishing-style kayak. Continuous point measurements were collected by turning on the sonar at the top of each reach and floating downstream using a consistent, zig-zag pattern from bank-to-bank along the entire length of the reach. Coordinates for the top and bottom of each reach and sonar start and end times were manually recorded. HOBO level loggers mounted on a meter stick were used to record depth in reach sections too shallow to collect accurate sonar data. Mean channel width for non-wadeable rivers where depth data was collected using sonar was calculated for each reach by averaging a minimum of five width estimates from the sonar map. For two sites on the Naches River, WA, river depth and channel width were determined from a rating curve developed by the Washington Department of Ecology (https://apps.ecology.wa.gov/publications/SummaryPages/1803009.html). For three sites on the Yakima River, river depth and channel width were determined from a rating curve developed using data from the United States Geological Survey (USGS) gauging station at Union Gap, Kiona and Mabton.

Stream discharge and velocity for each site were extracted from the National Oceanic and Atmospheric Administration (NOAA) National Water Model Retrospective Dataset Version 2.1 (NWM V2.1; https://registry.opendata.aws/nwm-archive/). This dataset provides a 42-y (February 1979 through December 2020) hourly simulation at all sampling locations. We computed the August monthly average discharge and velocity across these simulation years as input variables for determining an estimate of gas exchange rate (K600*)* for streamMetabolizer model runs (Section 5). Median grain size (d50) data for all the sites were extracted from NEXSS[10] which uses d50 data from the National Rivers and Streams Assessment and the Wadeable Stream Assessment (https://www.epa.gov/national-aquatic-resource-surveys/nrsa).

4. Surface water sampling

During the week of August 8–11, 2022, surface water samples were collected in triplicate from each site for different analysis. A set of samples were collected using a 50-mL syringe and filtered into 40-mL amber glass vials (ThermoScientific™ Amber Clean Snap Vials) using a 0.22-µm sterivex filter (MilliporeSigmaTM Sterivex™ Sterile Pressure-Driven Devices; MilliporeSigmaTM; Burlington, Massachusetts, USA). Filtered samples were analyzed for dissolved organic carbon (DOC) and total dissolved nitrogen (TDN). Additionally, one unfiltered water sample was collected using a pre-washed 2-L amber bottle (Nalgene™ Rectangular Amber HDPE Bottles; ThermoFisher Scientific; Waltham, Massachusetts, USA) for total suspended solids (TSS). All samples were stored on ice in the field and then refrigerated at 4° C before shipping for analysis at the Pacific Northwest National Laboratory (PNNL) Marine and Coastal Research Laboratory in Sequim, Washington (DOC, TDN) or transported to PNNL Biological Sciences Facility Laboratory in Richland, Washington (TSS). TSS samples were analyzed within one week of collection and DOC and TDN content were measured within two weeks of collection.

Dissolved organic carbon (DOC) and TDN were measured using a Shimadzu TOC-L Total Organic Carbon Analyzer. DOC was measured as non-purgeable organic carbon and TDN was measured by converting nitrogen in the samples to nitrogen gas and detected via chemiluminescence. Visual checks of calibration curves, samples, blanks, and check standard

peaks were performed before exporting data. Concentrations below the limit of detection (LOD) of the instrument, or below the standard curve, were flagged[73]. The LOD for DOC was 0.17-0.51 mg C L^{-1} and the LOD for TDN was 0.027 mg N L^{-1}. If the concentration of an analyte was below the lowest standard but above the LOD, the flag for that sample was replaced with half of the concentration of the lowest standard. If the analyte was below the LOD, the flag for that sample was replaced with a value corresponding to half of the LOD for that run. The coefficient of variation (CV) for each replicate set was calculated. Replicates with CV of 30 % or higher were flagged and the outlier sample was identified by calculating the distance between each of the replicate samples. Replicates with the highest distance to the other two replicates were flagged as outliers and removed from the analysis. Mean values for each site were then calculated from the remaining replicates and inputted as predictor variables in the regression analysis (Section 8).

Total suspended solids (TSS) samples were filtered in the laboratory through a pre-weighed and pre-combusted 4.7 cm, 0.7 µm GF/F glass microfiber filter (Whatman™ glass microfiber filters, Grade 934-AH®; MilliporeSigma; Burlington, Massachusetts, USA). After water filtration, the filter and filtration apparatus were rinsed with 30 mL of ultrapure Milli-Q water (Milli-Q® IQ Water Purification System; MilliporeSigma; Burlington, Massachusetts, USA) to ensure that all residue was captured by the filter. The filter was placed in foil and oven dried overnight at 45° C. The filter was allowed to cool in a desiccator prior to weighing. TSS was calculated as the difference between the weight of the filter before and after filtration of the water sample divided by the volume of water filtered[74]. Similar to the approach applied to DOC/TN, if the TSS of a sample was below the LOD, the flag for that sample was replaced with a value corresponding to half of the LOD (TSS LOD = 0.24 mg L^{-1}) for the TSS method.

5. Total Ecosystem Respiration (ER_{tot}) estimates

We estimated ER_{tot} using the streamMetabolizer R package[27] which estimates ER, GPP and gas exchange (K600) as parameters fit to a diel model of dissolved oxygen. Model inputs consisted of time series data for DO, water temperature, barometric pressure (BP), adjusted time series of depth (Supplementary methods), site ID, site latitude and longitude and a site-specific prior estimate of gas exchange rate coefficient (K600, day^{-1}). Gas exchange normalized to a Schmidt number of 600 (K600, day^{-1}) is a free parameter estimated within streamMetabolizer via Bayesian inference and therefore requires a prior probability estimate. We first estimated a prior k600 (m day^{-1}) value using the empirical relationship described in Model Equation 7 from Table 2 in Raymond et al. (2012)[75] as well as site specific slope, discharge, and velocity (Section 1 and 3). k600 values were then divided by the reach-averaged depth (Supplementary methods) to obtain a prior probability estimate for K600.

Before running the model, the 15-min time series BP and reach-averaged depth were interpolated (zoo::na.approx function)[76] to match the time interval of the water temperature and DO. Then the temperature, DO, and BP 1-min time series data were down-sampled to a 15-min resolution. Down-sampling improved both solution time and K600 pooling. DO time series was visually inspected and days with odd DO signals or biofouling were removed from the timeseries prior running the model. Additionally, we flagged and interpolated outliers in the DO time series using the R function 'auto_data_cleaning' within the 'tsrobprep' package[77] and used interquartile range for outlier detection. Further, photosynthetically active radiation (PAR) was estimated using the streamMetabolizer::calc_light() function[27], which is based on solar time, latitude, and longitude. Saturated DO concentration was calculated for each DO time series using water temperature and BP times series data and the Garcia and Gordon (1992)[78] equation (streamMetabolizer::calc_DO_sat function)[27].

For most of the sites, the Bayesian model was configured with normal K600 pooling, which is to say we partially pooled daily log K600 estimates in a Bayesian multilevel model. We also used the state-space option in streamMatbolizer to estimate observation and process error for dissolved O_2. The prior for K600 (K600_daily_meanlog_meanlog) was set as the natural log of the K600 prior estimate and a K600 scale value of 0.7. Group level variation in log K600 was K600~normal (0,0.05). We estimated posterior probability distribution for parameters via Hamiltonian Monte Carlo using the program Stan with 2000 warm-up steps, and 2000 saved steps across four chains. Some sites failed to converge with the settings mentioned, thus the K600 daily sigma prior was changed to 0.08, 0.02, 0.01 or 0.05 depending on the site. StreamMetabolizer outputs comprised ER_{tot} (g O_2 m^{-2} day^{-1}), GPP (g O_2 m^{-2} day^{-1}), and K600 (day^{-1}) as mean daily estimates over the number of days with quality DO data over deployment time[79]. Finally, we calculated the mean GPP and ER_{tot} for the entire deployment time for each site.

6. Water column respiration (ER_{wc}) and sediment-associated respiration (ER_{sed}) estimates

We estimated water column respiration in triplicate for 75 min at each site during sampling week using the *in situ* dark bottle incubation approach previously described by Laan et al. (2025)[35]. Briefly, a DO sensor (miniDOT Logger; Precision Measurement Engineering, Inc., Vista, CA, USA) and a small, battery-powered mixing device (i.e., toy boat motor propellor) were placed inside a 2-L dark bottle in triplicate (Nalgene™ Rectangular Amber HDPE bottles; ThermoFisher Scientific, Waltham, Massachusetts, USA). DO sensors and mixing devices were placed in a cooler with blue ice packs to keep them cool and minimize the time needed at each site for the sensors to equilibrate with river water temperatures. Bottles with the sensor and mixing device were rinsed three times with river water, and filled with river water from the thalweg, ensuring no air bubbles were trapped inside. Once full, the bottles were deployed on the riverbed as close to the thalweg as possible, depending on river depth and access to the shoreline, and weighted down with bricks or larger rocks. The sensors recorded DO concentration and temperature at 1-min intervals during the 75-min incubation period.

We extracted the raw DO and temperature sensor data for each site and plotted each variable against incubation time for each set of triplicate incubations (n = 144). The plots were visually inspected to a) confirm that temperature sensors were at equilibrium with the river temperature when the 75-min incubation test period began and b) identify data gaps, outliers, and other data anomalies. Following the visual inspection of plots, we applied the DO correction factor (as described in Supplementary Methods), removed the first 5 minutes and trimmed the time-series to 70 min to account for data anomalies due to emptying and refreshing river water in the bottles at the beginning and end of the incubation period, and to ensure all sites had the same incubation time.

Water column respiration rates (ER_{wc}) for individual triplicate incubation samples were calculated as the slope of the linear regression model (R stats::lm function)[80] between DO and incubation time in units of day^{-1}. The volumetric daily rate was then converted to daily areal units (g O_2 m^{-2} day^{-1}) by multiplying by the reach-averaged depth (Supplementary methods). Only sample observations with a normalized root mean square error (NRMSE) ≤ 0.03 were used for further analysis[81]. Although all triplicate samples met the NRMSE criteria, we removed a replicate from two sites after visual inspection due to the curve deviating from the other two replicates. Furthermore, six additional sites only had two replicates due to sensor or data loss. Median, mean, and range of ER_{wc} values for each site were calculated. 40% of ER_{wc} values were slightly positive (i.e., $ER_{wc} > 0$). Although positive respiration rates are biologically

unrealistic, and values greater than 0 g O_2 m^{-2} day^{-1} but less than 0.5 g O_2 m^{-2} day^{-1} are difficult to distinguish from zero, we retained positive ER_{wc} values to prevent biasing the data.

Sediment-associated respiration (ER_{sed}) estimates were performed by combining streamMetabolizer outputs of mean total ecosystem respiration (ER_{tot}) with in situ dark bottle incubations to isolate water column respiration (ER_{wc}). Respiration directly and indirectly associated with sediments (ER_{sed}) was found by the difference between ER_{tot} and ER_{wc}, assuming zero ER_{wc} if the estimated values were positive. These, ER_{sed} estimates include sediment-associated respiration from all ecosystem components besides the water column.

7. Model-predicted hyporheic zone respiration

Model-predicted HZ respiration values were previously published in Son et al., (2022)[13], and the data is publicly available on ESS-DIVE[82]. Respiration values by Son et al. (2022)[13] correspond to the amount of oxygen respiration in the HZ via vertical and lateral hyporheic exchange between the stream and the HZ, respectively. Therefore, total model-predicted HZ respiration is a sum of vertical and lateral respiration. The respiration is scaled by the stream surface area. Respiration values reported in Son et al., (2023)[82] in units of mol O_2 day^{-1}, were converted to g O_2 m^{-2} day^{-1} using the molar mass of oxygen and RCM stream reach area. We note that model outputs cover only 46 out of the 48 sites that we studied in the YRB.

8. Data analysis

To explore how physical variables covary with in ER_{sed} at different sites, a LASSO (Least Absolute Shrinkage and Selection Operator) regression model was built using physical, chemical and environmental variables (Table 4) as inputs, and ER_{sed} as the target variable. Prior to conducting the LASSO regression, variables were cube root transformed to reduce the impact of high leverage points in the regression analysis. Additionally, standardization was applied to achieve a mean of zero and standard deviation of 1 (i.e. z-score) for all variable to ensure that each variable is equally and fairly treated without penalizing a variable simply due to the magnitude or scale of its nature. The LASSO regression was performed over 100 random seeds. β coefficients were normalized to the maximum β coefficient for each regression, then averaged over the 100 random seeds for the final, reported value. Both the raw and normalized mean β coefficient and standard deviation are reported in addition to the R^2.

To investigate the correlation between RCM-predicted HZ respiration and field-estimated ER_{tot} and ER_{sed}, Pearson as well as Spearman's rank correlation were used. In this study, we used Pearson correlation to investigate the correlation between the z-score normalized RCM-predicted HZ respiration and ER_{tot}/ER_{sed} (with mean of zero, standard deviation of one), and Spearman's rank-order correlation to investigate their rank-order correlation. Linear regression analyses were performed using the 'lm' function in the base R package. All analyses were performed using R Statistical Software (v4.1.3)[80].

Table 4. Variables used as inputs in the LASSO regression model. All NHDPlus, StreamCat, NLCD, and ET0 database data were extracted using the custom R script[68].

Variable	Description	Unit	Data Source	Data Source Citation
Water Temperature	HOBO water temperature	C°	Field measured	Delgado et al. (2023)[74]
Mean Depth	average water depth	cm	Field estimated	Delgado et al. (2023)[74]
Slope	stream slope	NA	NHDPlus	McKay et al. (2012)[70]
Velocity	stream velocity	$m\ s^{-1}$	National Water Model	Cosgrove et al. (2024)[83]
Discharge	Discharge	$m^3\ s^{-1}$	National Water Model	Cosgrove et al. (2024)[83]
Dissolved Organic Carbon	non-purgeable organic carbon	$mg\ L^{-1}$	Field measured	Forbes et al. (2023)[73]
Total Dissolved Nitrogen	total dissolved nitrogen	$mg\ L^{-1}$	Field measured	Forbes et al. (2023)[73]
Total Suspended Solids	total suspended solids	$mg\ L^{-1}$	Field measured	Delgado et al. (2023)[74]
Drainage Area	total drainage area	km^2	NHDPlus	McKay et al. (2012)[70]
Percent Forest Cover	percentage of forest as the sum of percentage deciduous, coniferous and mixed forest	%	StreamCat and NLCD	Hill et al. (2016)[69] Jin et al. (2023)[84]
Percent Agricultural Cover	percentage agriculture as the sum of percentage crop and hay	%	StreamCat and NLCD	Hill et al. (2016)[69] Jin et al. (2023)[84]
Percent Shrub Cover	Percentage Shrub	%	StreamCat and NLCD	Hill et al. (2016)[69] Jin et al. (2023)[84]
Aridity	Aridity	NA	ET0 Database	Zomer et al. (2012)[85]
Median grain size (d50)	median grain size	m	National Rivers and Streams Assessment and the Wadeable Stream Assessment	Kaufman et al. (2023)[79]
Gross Primary Production (GPP)	gross primary production	$gO_2\ m^{-2}{\cdot}day^{-1}$	streamMetabolizer output	Kaufman et al. (2023)[79]

Data Availability:

Data collected in the field were published previously in Forbes et al. (2023)[73] and Delgado et al. (2023)[74]. Data generated as part of this manuscript is currently available on GitHub (see below) and will be published on the Environmental System Science Data Infrastructure for a Virtual Ecosystem (ESS-DIVE) repository upon manuscript acceptance. ESS-DIVE repositories and are licensed for reuse under the Creative Commons Attribution 4.0 International License.

Code Availability

Scripts necessary to reproduce the primary results of this article are available at https://github.com/river-corridors-sfa/SSS_metabolism.

References:

1. Battin, T. J. *et al.* River ecosystem metabolism and carbon biogeochemistry in a changing world. *Nature* **613**, 449–459 (2023).
2. Naegeli, M. W. & Uehlinger, U. Contribution of the Hyporheic Zone to Ecosystem Metabolism in a Prealpine Gravel-Bed-River. *Journal of the North American Benthological Society* **16**, 794–804 (1997).
3. Battin, T. J., Kaplan, L. A., Newbold, J. D. & Hendricks, S. P. A mixing model analysis of stream solute dynamics and the contribution of a hyporheic zone to ecosystem function*. *Freshwater Biology* **48**, 995–1014 (2003).
4. Gagne-Maynard, W. C. *et al.* Evaluation of Primary Production in the Lower Amazon River Based on a Dissolved Oxygen Stable Isotopic Mass Balance. *Front. Mar. Sci.* **4**, (2017).
5. Fuss, C. & Smock, L. Spatial and temporal variation of microbial respiration rates in a blackwater stream. *Freshwater Biology* **36**, 339–349 (1996).
6. Kaplan, L. A. & Newbold, J. D. 10 - Surface and Subsurface Dissolved Organic Carbon. in *Streams and Ground Waters* (eds. Jones, J. B. & Mulholland, P. J.) 237–258 (Academic Press, San Diego, 2000). doi:10.1016/B978-012389845-6/50011-9.
7. Jones, J. Factors controlling hyporheic respiration in a desert stream. *Freshwater Biology* **34**, 91–99 (1995).
8. Pusch, M. & Schwoerbel, J. Community respiration in hyporheic sediments of a mountain stream (Steina, Black Forest). *Archiv fur Hydrobiologie* **130**, 35–35 (1994).
9. Fellows, C. S., Valett, M. H. & Dahm, C. N. Whole-stream metabolism in two montane streams: Contribution of the hyporheic zone. *Limnology and Oceanography* **46**, 523–531 (2001).
10. Gomez-Velez, J. D., Harvey, J. W., Cardenas, M. B. & Kiel, B. Denitrification in the Mississippi River network controlled by flow through river bedforms. *Nature Geosci* **8**, 941–945 (2015).
11. Fang, Y. *et al.* High-Performance Simulation of Dynamic Hydrologic Exchange and Implications for Surrogate Flow and Reactive Transport Modeling in a Large River Corridor. *Frontiers in Water* **2**, (2020).
12. Fang, Y. *et al.* A multirate mass transfer model to represent the interaction of multicomponent biogeochemical processes between surface water and hyporheic zones (SWAT-MRMT-R 1.0). *Geoscientific Model Development* **13**, 3553–3569 (2020).
13. Son, K., Fang, Y., Gomez-Velez, J. D. & Chen, X. Spatial Microbial Respiration Variations in the Hyporheic Zones Within the Columbia River Basin. *Journal of Geophysical Research: Biogeosciences* **127**, (2022).
14. Odum, H. T. Primary Production in Flowing Waters. *Limnology and Oceanography* **1**, 102–117 (1956).
15. Hall, R. O. & Hotchkiss, E. R. Chapter 34 - Stream Metabolism. in *Methods in Stream Ecology (Third Edition)* (eds. Lamberti, G. A. & Hauer, F. R.) 219–233 (Academic Press, 2017). doi:10.1016/B978-0-12-813047-6.00012-7.
16. Kaylor, M. J., White, S. M., Saunders, W. C. & Warren, D. R. Relating spatial patterns of stream metabolism to distributions of juveniles salmonids at the river network scale. *Ecosphere* **10**, e02781 (2019).
17. Hotchkiss, E. R. *et al.* Sources of and processes controlling CO2 emissions change with the size of streams and rivers. *Nature Geosci* **8**, 696–699 (2015).
18. O'Donnell, B. & Hotchkiss, E. R. Resistance and resilience of stream metabolism to high flow disturbances. *Biogeosciences* **19**, 1111–1134 (2022).
19. Gómez-Gener, L. *et al.* Towards an improved understanding of biogeochemical processes across surface-groundwater interactions in intermittent rivers and ephemeral streams. *Earth-Science Reviews* **220**, 103724 (2021).

20. Bernot, M. J. *et al.* Inter-regional comparison of land-use effects on stream metabolism. *Freshwater Biology* **55**, 1874–1890 (2010).
21. Song, C. *et al.* Continental-scale decrease in net primary productivity in streams due to climate warming. *Nature Geosci* **11**, 415–420 (2018).
22. Arroita, M., Elosegi, A. & Hall Jr., R. O. Twenty years of daily metabolism show riverine recovery following sewage abatement. *Limnology and Oceanography* **64**, S77–S92 (2019).
23. Tromboni, F. *et al.* High rates of daytime river metabolism are an underestimated component of carbon cycling. *Commun Earth Environ* **3**, 1–10 (2022).
24. Marzolf, N. S. & Ardón, M. Ecosystem metabolism in tropical streams and rivers: a review and synthesis. *Limnology and Oceanography* **66**, 1627–1638 (2021).
25. Bernhardt, E. S. *et al.* Light and flow regimes regulate the metabolism of rivers. *Proceedings of the National Academy of Sciences* **119**, e2121976119 (2022).
26. Gurung, A., Iwata, T., Nakano, D. & Urabe, J. River Metabolism along a Latitudinal Gradient across Japan and in a global scale. *Sci Rep* **9**, 4932 (2019).
27. Appling, A. P., Hall, R. O., Yackulic, C. B. & Arroita, M. Overcoming Equifinality: Leveraging Long Time Series for Stream Metabolism Estimation. *Journal of Geophysical Research: Biogeosciences* **123**, 624–645 (2018).
28. Hall Jr, R. O., Kennedy, T. A. & Rosi-Marshall, E. J. Air–water oxygen exchange in a large whitewater river. *Limnology and Oceanography: Fluids and Environments* **2**, 1–11 (2012).
29. Hall Jr., R. O. *et al.* Turbidity, light, temperature, and hydropeaking control primary productivity in the Colorado River, Grand Canyon. *Limnology and Oceanography* **60**, 512–526 (2015).
30. Roche, K. R. & Dentz, M. Benthic Biolayer Structure Controls Whole-Stream Reactive Transport. *Geophysical Research Letters* **49**, e2021GL096803 (2022).
31. Schindler, D. E., Jankowski, K., A'mar, Z. T. & Holtgrieve, G. W. Two-stage metabolism inferred from diel oxygen dynamics in aquatic ecosystems. *Ecosphere* **8**, e01867 (2017).
32. Hotchkiss, E. R. & Hall, Jr., Robert O. High rates of daytime respiration in three streams: Use of δ18OO2 and O2 to model diel ecosystem metabolism. *Limnology and Oceanography* **59**, 798–810 (2014).
33. del Giorgio, P. A., Cole, J. J. & Cimbleris, A. Respiration rates in bacteria exceed phytoplankton production in unproductive aquatic systems. *Nature* **385**, 148–151 (1997).
34. Appling, A. P. *et al.* The metabolic regimes of 356 rivers in the United States. *Scientific Data* **5**, 180292 (2018).
35. Laan, M. *et al.* Water Column Respiration in the Yakima River Basin is Explained by Temperature, Nutrients and Suspended Solids. *EGUsphere* **2025**, (2025).
36. Ward, N. D. *et al.* Velocity-amplified microbial respiration rates in the lower Amazon River. *Limnology and Oceanography Letters* **3**, 265–274 (2018).
37. Ward, N. D., Sawakuchi, H. O., Richey, J. E., Keil, R. G. & Bianchi, T. S. Enhanced Aquatic Respiration Associated With Mixing of Clearwater Tributary and Turbid Amazon River Waters. *Front. Earth Sci.* **7**, (2019).
38. Reisinger, A. J. *et al.* Water column contributions to the metabolism and nutrient dynamics of mid-sized rivers. *Biogeochemistry* **153**, 67–84 (2021).
39. Ellis, E. E. *et al.* Factors controlling water-column respiration in rivers of the central and southwestern Amazon Basin. *Limnology and Oceanography* **57**, 527–540 (2012).
40. Reisinger, A. J., Tank, J. L., Rosi-Marshall, E. J., Hall, R. O. & Baker, M. A. The varying role of water column nutrient uptake along river continua in contrasting landscapes. *Biogeochemistry* **125**, 115–131 (2015).
41. Reisinger, A. J., Tank, J. L., Hoellein, T. J. & Hall, R. O. Sediment, water column, and open-channel denitrification in rivers measured using membrane-inlet mass spectrometry. *Journal of Geophysical Research: Biogeosciences* **121**, 1258–1274 (2016).

42. del Giorgio, P. A. & Williams, P. J. le B. *Respiration in Aquatic Ecosystems*. (Oxford University Press, Oxford, United Kingdom, 2005).
43. Gardner, J. R. & Doyle, M. W. Sediment–Water Surface Area Along Rivers: Water Column Versus Benthic. *Ecosystems* **21**, 1505–1520 (2018).
44. Newcomer, M. E. *et al.* Influence of Hydrological Perturbations and Riverbed Sediment Characteristics on Hyporheic Zone Respiration of CO2 and N2. *Journal of Geophysical Research: Biogeosciences* **123**, 902–922 (2018).
45. Roche, K. R. *et al.* Benthic biofilm controls on fine particle dynamics in streams. *Water Resources Research* **53**, 222–236 (2017).
46. Krause, S. *et al.* Ecohydrological interfaces as hot spots of ecosystem processes. *Water Resources Research* **53**, 6359–6376 (2017).
47. Roley, S. S., Hall Jr., R. O., Perkins, W., Garayburu-Caruso, V. A. & Stegen, J. C. Coupled primary production and respiration in a large river contrasts with smaller rivers and streams. *Limnology and Oceanography* **n/a**, 15 (2023).
48. Hall, R. O., Tank, J. L., Baker, M. A., Rosi-Marshall, E. J. & Hotchkiss, E. R. Metabolism, Gas Exchange, and Carbon Spiraling in Rivers. *Ecosystems* **19**, 73–86 (2016).
49. Battin, T. J., Kaplan, L. A., Newbold, J. D., Cheng, X. & Hansen, C. Effects of Current Velocity on the Nascent Architecture of Stream Microbial Biofilms. *Appl Environ Microbiol* **69**, 5443–5452 (2003).
50. Cohen, S., Wan, T., Islam, M. T. & Syvitski, J. Global river slope: A new geospatial dataset and global-scale analysis. *Journal of hydrology* **563**, 1057–1067 (2018).
51. Anderton, C. R. *et al.* Nitrogen Source Governs Community Carbon Metabolism in a Model Hypersaline Benthic Phototrophic Biofilm. *mSystems* **5**, e00260-20 (2020).
52. Duarte, C. M. & Prairie, Y. T. Prevalence of Heterotrophy and Atmospheric CO2 Emissions from Aquatic Ecosystems. *Ecosystems* **8**, 862–870 (2005).
53. Munn, M. D., Konrad, C. P., Miller, M. P. & Jaeger, K. A comparison of spatial and temporal drivers of stream metabolism. *Freshwater Biology* **68**, 1751–1764 (2023).
54. Carter, A. M. *et al.* Exceptions to the Heterotrophic Rule: Prevalence and Drivers of Autotrophy in Streams and Rivers. *Ecosystems* **27**, 969–985 (2024).
55. Griffiths, N. A. *et al.* Agricultural land use alters the seasonality and magnitude of stream metabolism. *Limnology and Oceanography* **58**, 1513–1529 (2013).
56. Summers, B. M. *et al.* Long-term data reveal highly-variable metabolism and transitions in trophic status in a montane stream. *Freshwater Science* **39**, 241–255 (2020).
57. Young, R. G. & Huryn, A. D. Effects of Land Use on Stream Metabolism and Organic Matter Turnover. *Ecological Applications* **9**, 1359–1376 (1999).
58. Hoellein, T. J., Bruesewitz, D. A. & Richardson, D. C. Revisiting Odum (1956): A synthesis of aquatic ecosystem metabolism. *Limnology and Oceanography* **58**, 2089–2100 (2013).
59. Fazekas, H. M., McDowell, W. H., Shanley, J. B. & Wymore, A. S. Climate Variability Drives Watersheds Along a Transporter-Transformer Continuum. *Geophysical Research Letters* **48**, e2021GL094050 (2021).
60. Price, A. N. *et al.* Biogeochemical and community ecology responses to the wetting of non-perennial streams. *Nat Water* **2**, 815–826 (2024).
61. Ejarque, E. *et al.* Climate-induced hydrological variation controls the transformation of dissolved organic matter in a subalpine lake. *Limnology and Oceanography* **63**, 1355–1371 (2018).
62. Rehage, H. & Kind, M. The first Damköhler number and its importance for characterizing the influence of mixing on competitive chemical reactions. *Chemical Engineering Science* **229**, 116007 (2021).
63. McClain, M. E. *et al.* Biogeochemical hot spots and hot moments at the interface of terrestrial and aquatic ecosystems. *Ecosystems* 301–312 (2003).

64. Bernhardt, E. S. *et al.* Control Points in Ecosystems: Moving Beyond the Hot Spot Hot Moment Concept. *Ecosystems* **20**, 665–682 (2017).
65. Qiu, J. *et al.* Implications of water management representations for watershed hydrologic modeling in the Yakima River basin. *Hydrology and Earth System Sciences* **23**, 35–49 (2019).
66. Vaccaro, J. J. & Olsen, T. D. *Estimates of Ground-Water Recharge to the Yakima River Basin Aquifer System, Washington, for Predevelopment and Current Land-Use and Land-Cover Conditions*. (2007).
67. Vano, J. A. *et al.* Climate change impacts on water management and irrigated agriculture in the Yakima River Basin, Washington, USA. *Climatic Change* **102**, 287–317 (2010).
68. Willi, K. & Ross, M. R. V. Geospatial Data Puller for Waters in the Contiguous United States (Version v1). (2023).
69. Hill, R. A., Weber, M. H., Leibowitz, S. G., Olsen, A. R. & Thornbrugh, D. J. The Stream-Catchment (StreamCat) Dataset: A Database of Watershed Metrics for the Conterminous United States. *JAWRA Journal of the American Water Resources Association* **52**, 120–128 (2016).
70. McKay, L. *et al. NHDPlus Version 2: User Guide*. (2012).
71. Zomer, R. & Trabucco, A. Global Aridity Index and Potential Evapotranspiration (ET0) Database: Version 3. 6086884631 Bytes [object Object] https://doi.org/10.6084/M9.FIGSHARE.7504448.V6 (2022).
72. Hijmans, R. J., Bivand, R., Pebesma, E. & Sumner, M. D. terra: Spatial Data Analysis. (2024).
73. Forbes, B. *et al.* WHONDRS River Corridor Dissolved Oxygen, Temperature, Sediment Aerobic Respiration, Grain Size, and Water Chemistry from Machine-Learning-Informed Sites across the Contiguous United States (v3). [object Object] https://doi.org/10.15485/1923689 (2023).
74. Delgado, D. *et al.* Spatial Study 2022: Surface Water Samples, Cotton Strip Degradation, and Hydrologic Sensor Data across the Yakima River Basin, Washington, USA (v2). (2023).
75. Raymond, P. A. *et al.* Scaling the gas transfer velocity and hydraulic geometry in streams and small rivers. *Limnology and Oceanography: Fluids and Environments* **2**, 41–53 (2012).
76. Zeileis, A. & Grothendieck, G. **zoo** : *S3* Infrastructure for Regular and Irregular Time Series. *J. Stat. Soft.* **14**, (2005).
77. Narajewski, M., Kley-Holsteg, J. & Ziel, F. tsrobprep — an R package for robust preprocessing of time series data. *SoftwareX* **16**, 100809 (2021).
78. Garcia, H. E. & Gordon, L. I. Oxygen solubility in seawater: Better fitting equations. *Limnol. Oceanogr.* **37**, 1307–1312 (1992).
79. Kaufman, M. H. *et al.* Spatial Study 2022: Water Column, Sediment, and Total Ecosystem Respiration Rates across the Yakima River Basin, Washington, USA. (2023).
80. R Core Team. R: The R Project for Statistical Computing. R Foundation for Statistical Computing (2022).
81. Shcherbakov, M. V. *et al.* A survey of forecast error measures. *World applied sciences journal* **24**, 171–176 (2013).
82. Son, K., Fang, Y., Gomez-Velez, J. D. & Chen, X. Model Inputs, Outputs, and Scripts associated with: “Spatial microbial respiration variations in the hyporheic zones within the Columbia River Basin”. [object Object] https://doi.org/10.15485/1962818 (2023).
83. Cosgrove, B. *et al.* NOAA’s National Water Model: Advancing operational hydrology through continental-scale modeling. *J American Water Resour Assoc* 1752–1688.13184 (2024) doi:10.1111/1752-1688.13184.
84. Jin, S. *et al.* National Land Cover Database 2019: A Comprehensive Strategy for Creating the 1986–2019 Forest Disturbance Product. *J Remote Sens* **3**, 0021 (2023).

85. Zomer, R. J., Xu, J. & Trabucco, A. Version 3 of the Global Aridity Index and Potential Evapotranspiration Database. *Sci Data* **9**, 409 (2022).

Acknowledgements:
This work was supported by the River Corridor Science Focus Area (SFA) at the Pacific Northwest National Laboratory (PNNL). The SFA is supported by the United States Department of Energy, Office of Biological and Environmental Research (BER), Environmental System Science (ESS) Program. PNNL is operated by Battelle Memorial Institute for the United States Department of Energy under contract no. DE-AC05-76RL01830. We thank the United States Forest Service, Washington Department of Natural Resources, Washington Department of Fish and Wildlife, Confederated Tribes and Bands of the Yakama Nation, and Cowiche Canyon Conservancy for access to field locations where these samples were collected. We also thank the Confederated Tribes and Bands of the Yakama Nation Tribal Council and Yakama Nation Fisheries for working with us to facilitate sample collection and optimization of data usage according to their values and worldview. We thank the field team including: Dillman Delgado, Morgan Barnes, Brandon T. Boehnke, Yunxiang Chen, Kali Cornwell, Brianna I. Gonzalez, Samantha Grieger, Glenn E. Hammond, Peishi Jiang, Bing Li, Zhi Li, Xinming Lin, Sophia A. McKever, Maruti K. Mudunuru, Katherine A. Muller, Opal Otenburg, Aaron Pelly, Kelsey Peta, Alan Roebuck, Joshua M. Torgeson, and Jianqiu Zheng.

Author Contributions:
VAGC, MK, BH and JCS conceptualized the study. JCS, LR, SF, ML conducted the field work. LR and ML analyzed samples. KS, XC and YF configured RCM outputs for this study. XL, ML and BF processed the data and performed analyses with feedback from VAGC, MK, MK, BH and JCS. VAGC and MK carried out metabolism analysis with feedback from BH. BF managed the data. VAGC, MK, SF, BF and JCS drafted the initial manuscript, and all authors contributed to revisions.

Competing interests
All authors declare that there are no competing interests.